AGU PUBLICATIONS

Geophysical Research Letters

RESEARCH LETTER
10.1002/2017GL073989

Key Points:
- Variation in trench retreat velocity controls the observed slab morphology in Izu-Bonin subduction zone
- The 30 May 2015 Bonin Islands earthquake may be explained as the result of Pacific slab buckling due to slow trench retreat
- Subducted slab is inherently heterogeneous due to nonlinear viscosity, contributing to the occurrences of isolated deep earthquakes

Supporting Information:
- Supporting Information S1
- Movie S1
- Movie S2

Correspondence to:
T. Yang,
tyang@gps.caltech.edu

Citation:
Yang, T., M. Gurnis, and Z. Zhan (2017), Trench motion-controlled slab morphology and stress variations: Implications for the isolated 2015 Bonin Islands deep earthquake, *Geophys. Res. Lett.*, *44*, 6641–6650, doi:10.1002/2017GL073989.

Received 29 APR 2017
Accepted 14 JUN 2017
Accepted article online 19 JUN 2017
Published online 3 JUL 2017

Trench motion-controlled slab morphology and stress variations: Implications for the isolated 2015 Bonin Islands deep earthquake

Ting Yang[1,2], Michael Gurnis[1], and Zhongwen Zhan[1]

[1]Seismological Laboratory, California Institute of Technology, Pasadena, California, USA, [2]Now at School of Earth Sciences, Melbourne University, Melbourne, Victoria, Australia

Abstract The subducted old and cold Pacific Plate beneath the young Philippine Sea Plate at the Izu-Bonin trench over the Cenozoic hosts regional deep earthquakes. We investigate slab morphology and stress regimes under different trench motion histories with mantle convection models. Viscosity, temperature, and deviatoric stress are inherently heterogeneous within the slab, which we link to the occurrence of isolated earthquakes. Models expand on previous suggestions that observed slab morphology variations along the Izu-Bonin subduction zone, exhibited as shallow slab dip angles in the north and steeper dip angles in the south, are mainly due to variations in the rate of trench retreat from the north (where it is fast) to the south (where it is slow). Geodynamic models consistent with the regional plate tectonics, including oceanic plate age, plate convergence rate, and trench motion history, reproduce the seismologically observed principal stress direction and slab morphology. We suggest that the isolated ~680 km deep, 30 May 2015 M_w 7.9 Bonin Islands earthquake, which lies east of the well-defined Benioff zone and has its principal compressional stress direction oriented toward the tip of the previously defined Benioff zone, can be explained by Pacific slab buckling in response to the slow trench retreat.

1. Introduction

Subduction of oceanic lithosphere brings cold, high-viscosity material into the higher temperature less viscous mantle. The old and cold Pacific Plate subducts beneath the younger Philippine Sea Plate at the Izu-Bonin trench and causes the generation of deep earthquakes (Figure 1). The Wadati-Benioff zone shape varies along the Izu-Bonin subduction zone, IBSZ. The slab dip angle is shallow and the slab flattens at ~500 km depth in the northern IBSZ, while the slab dip angle is steep in the southern IBSZ (Figure 1). The principal compressional stress direction (*P* axis of earthquake focal mechanism) in the deep continuous part of the slab mainly aligns with the Benioff zone shape, although with significant variations (Figures 1b–1e). Consistent with the deep earthquake distribution, tomographic models also indicate that the slab dip angle is small in northern IBSZ and is large in the south [*van der Hilst and Seno*, 1993; *Miller et al*., 2005; *Wei et al*., 2012; *Zhao et al*., 2017].

On 30 May 2015, a M_w 7.9 earthquake occurred beneath the Bonin Islands at ~680 km depth and ruptured a nearly horizontal plane [*Ye et al*., 2016]. This event is unusually deep and isolates from the background seismicity forming the Wadati-Benioff zone (Figure 1d), presenting an example of an isolated large deep earthquake [*Lundgren and Giardini*, 1994; *Frohlich*, 2006]. In contrast to previous deep earthquakes regionally that are mainly shallower than 550 km, the 2015 Bonin Island earthquake is much deeper and lies east of the main trend of the Benioff zone (Figure 1d), with its principal compressional stress direction approximately oriented toward the tip of the local Benioff zone [*Ye et al*., 2016]. It is still unclear whether this event occurred above or below the 660 km discontinuity [*Kuge*, 2016], which may have been depressed by the cold subducted slab to a depth greater than 680 km [*Porritt and Yoshioka*, 2016]. Under the implicit assumption that deep earthquakes occur in the cold slab core, *Ye et al.* [2016] proposed two possible scenarios for the event's large depth and isolation from the Wadati-Benioff zone: (1) a slab tear close to the event separating the gently dipping slab to the north and the steeply dipping slab to the south; (2) significant slab folding within the mantle transition due to resistance of the higher-viscosity lower mantle. *Okal and Kirby* [2016] suggested that a previously unknown fragment of fossil slab may be responsible for the surprising event location. On the other hand, based on modeling of strong high-frequency coda waves, *Takemura et al.* [2016] argued that the M_w 7.9 Bonin earthquake could be located near the bottom edge of the subducted slab, instead of near its center.

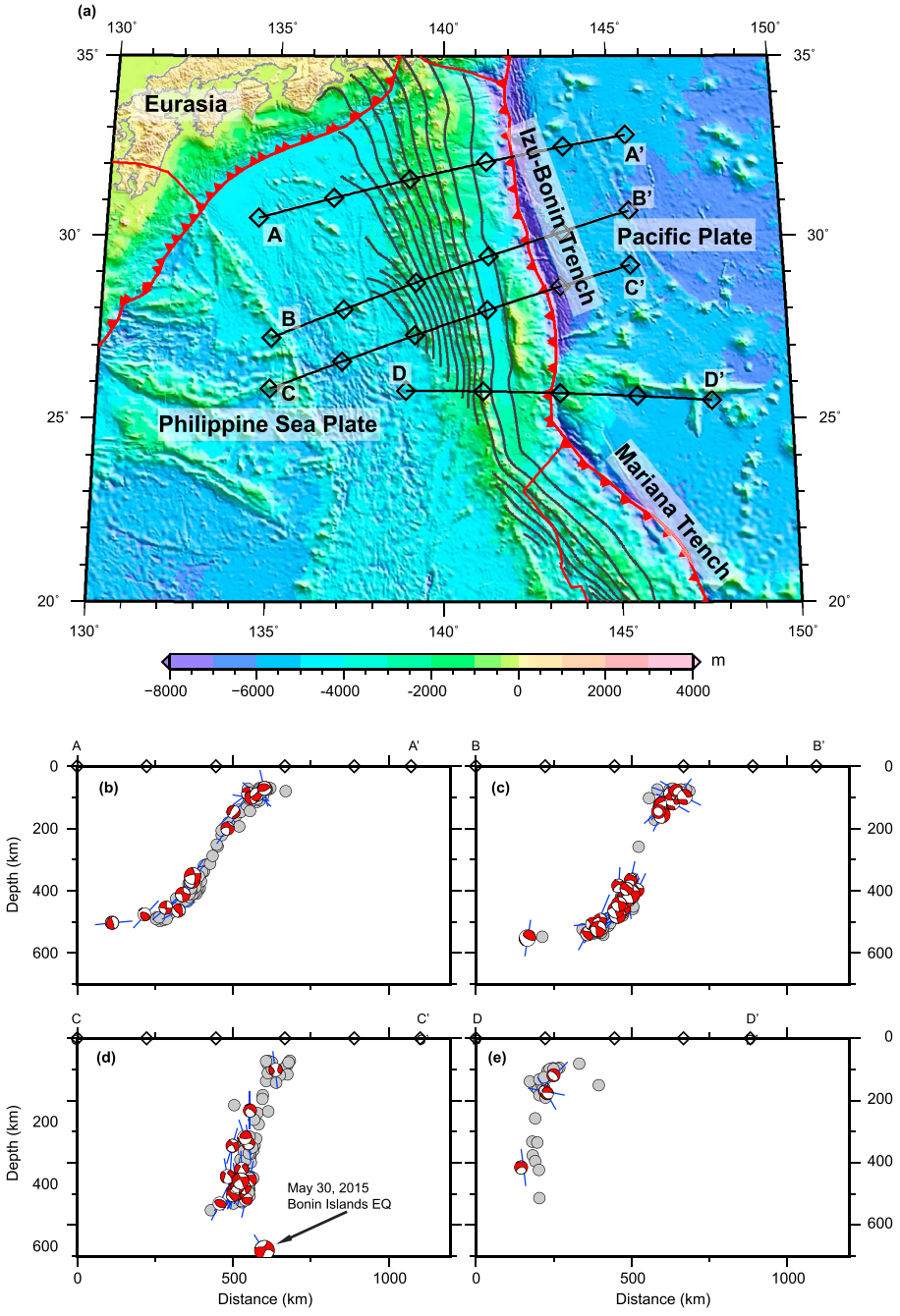

Figure 1. Benioff zone shape and deep earthquakes (below 70 km depth) focal mechanisms at the Izu-Bonin subduction zone. (a) Topography [*Amante and Eakins*, 2009] around the Izu-Bonin subduction zone. Red curved lines represent plate boundaries [*Bird*, 2003] with small red triangles at the subduction zones pointing to the overriding plate. Black curved lines represent slab interface depth from Slab 1.0 model [*Hayes et al.*, 2012]. (b–e) Deep earthquake distribution and focal mechanisms at different profiles along the Izu-Bonin subduction zone. The profile locations are plotted in Figure 1a. Gray circles represent deep earthquakes from the EHB catalogue [*Engdahl et al.*, 1998]. The global centroid moment tensor focal mechanisms are indicative of the 3-D principal stress directions. Projected compressional axes along each profile (blue line) are also plotted. In Figure 1d, the 30 May 2015 Bonin Islands deep earthquake is labeled.

Obayashi et al. [2017] proposed a similar explanation that the event occurred near the heel of a boot-like slab structure, before its penetration into the lower mantle. *Zhao et al.* [2017] suggested that the Pacific slab splits slightly north of the 2015 Bonin earthquake hypocenter which is within the subducting Pacific slab that is penetrating into the lower mantle.

The observed slab (Benioff zone) morphology variations along the IBSZ are qualitatively consistent with slab subduction numerical models with different trench motion histories. Numerical experiments suggest that trench motion history has a significant influence on slab deformation and stagnation within the transition zone [*Zhong and Gurnis*, 1995; *Christensen*, 1996; *Schellart*, 2005; *Faccenna et al*., 2009; *Stegman et al*., 2010; *Čížková and Bina*, 2013; *Agrusta et al*., 2017]. The retreat of the trench facilitates slab stagnation within the transition zone, lying subhorizontally. On the other hand, when the trench location is fixed or has a minor retreat with respect to the lower mantle, the slab is more prone to buckle and penetrate into the lower mantle [*Christensen*, 1996; *Čížková and Bina*, 2013]. Although substantial uncertainty exists in the reconstruction of the Philippine Sea Plate region, since it is mostly surrounded by subduction zones, several reconstructions suggest that the northern part of the IBSZ had significant retreat since the Oligocene (~30 Ma) while southern part of the IBSZ segment had much less retreat during the same period [*Hall*, 2002; *Miller et al*., 2006; *Faccenna et al*., 2009; *Von Hagke et al*., 2016; *Wu et al*., 2016].

We use geodynamic models to investigate slab morphology, temperature, stress regimes, and their evolution under different trench motion histories. We demonstrate that models consistent with regional plate tectonics can reproduce the observed slab morphology and deep earthquake *P* axis directions (assumed to be the principal compressional stress directions) regionally. We suggest that the location of the isolated 2015 Bonin Islands deep earthquake can be explained by the buckling of the Pacific slab beneath the Bonin Islands.

2. Method

We develop a model of plate subduction within a two-dimensional Cartesian geometry and investigate the influences of trench motion history on slab morphology and stress distribution. The equations governing mantle flow with prescribed initial and boundary conditions are solved with the finite element method using Citcom [*Moresi et al*., 1996; *Zhong*, 2006; *Leng and Zhong*, 2008]. The model domain is set as 2890 km in depth (from Earth's surface to core-mantle boundary (CMB)) and 5780 km in width and is divided into 832 equally spaced elements in the horizontal direction (element size 6.95 km) and into 192 uneven elements in the vertical direction. The vertical element size is 5 km in the uppermost mantle and gradually increases to 39.38 km in the lowermost mantle.

The surface is divided into two plates with the right old oceanic plate subducts beneath the left young oceanic plate at $X = 3800$ km (Figure S1 in the supporting information). The initial temperature field is based on a half-space cooling model (Figures S1b and S1c). The nondimensional temperature boundary conditions at the top and bottom boundaries are 0 and 1. In contrast to fully dynamic models [*Zhong and Gurnis*, 1995; *Yang et al*., 2016], the surface plates and trench motions are prescribed [*Christensen*, 1996] so that we can control these factors and investigate their influence on slab morphology and stress distribution. The velocity of trench retreat is set to the overriding plate velocity.

The viscosity is a composite of dislocation and diffusion creep and depends on depth, temperature, and strain rate [*Zhong and Gurnis*, 1995; *Yang et al*., 2016]:

$$\eta = \frac{\eta_{\mathrm{dif}}\eta_{\mathrm{dis}}}{\eta_{\mathrm{dif}} + \eta_{\mathrm{dis}}},$$

where η, η_{dif}, and η_{dis} represent a composite effective viscosity, viscosity via diffusion creep, and viscosity via dislocation creep, respectively. The diffusion creep viscosity is expressed as

$$\eta_{\mathrm{dif}} = \eta_0 \Gamma(x,z,t) \exp\left[E_0(T_0 - T) + 1.433 + 11.753z - 14.235z^2\right]$$

where η_0, E_0, and T_0 represent nondimensional viscosity prefactor, activation energy, and reference temperature in each layer; x, z, t, and T represent nondimensional horizontal and vertical coordinates, time and temperature, respectively. This viscosity setting leads to a high-viscosity lithosphere, low-viscosity asthenosphere, viscosity jump across the 660 km discontinuity, viscosity peak at ~2000 km, and gradual viscosity reduction to the CMB (Figure S1) as inferred previously from joint inversion of geophysical observations [*Mitrovica and Forte*, 2004]. $\Gamma(x,z,t)$ is a weak zone factor [*Hebert et al*., 2009; *Stadler et al*., 2010]. The weak zone sits above the subducted slab (Figure S1) and decouples the overriding and subducting plates

[*Zhong et al*., 1998; *van Hunen et al*., 2000], mimicking the dehydration-induced low-viscosity channel and localized sliding along thrust faults between the overriding and subducting plates. The weak zone changes its location and shape with time in response to mantle flow.

For simplicity, the nondimensional activation energy of dislocation creep is set to the same as the value for diffusion creep. Thus, the dislocation viscosity can be expressed as follows:

$$\eta_{\mathrm{dis}} = \left(\frac{\dot{\varepsilon}_0}{\dot{\varepsilon}_{II}}\right)^{1-1/n} {\eta_{\mathrm{dif}}}^{1/n},$$

where $\dot{\varepsilon}_{\mathrm{II}}$ and $\dot{\varepsilon}_0$ represent the second invariant of the strain rate and the reference strain rate, respectively; and n the nonlinear exponent for dislocation creep. The second invariant of the strain rate $\dot{\varepsilon}_{\mathrm{II}}$ is defined as $\dot{\varepsilon}_{\mathrm{II}} = \sqrt{\frac{1}{2}\left(\dot{\varepsilon}_{xx}^2 + \dot{\varepsilon}_{zz}^2 + 2\dot{\varepsilon}_{xz}^2\right)}$. In the lower mantle, n is 1 so the lower mantle flow is within the diffusion creep regime. Above 660 km depth, n is 3.5 so the dislocation creep viscosity is strongly nonlinear. To avoid problems with numerical convergence in response to the imposed surface velocity, n is set to 1 for the top 20 km.

The olivine to spinel phase transition at 410 km and the spinel to perovskite + magnoustite phase transition at 660 km depth are incorporated. The relative density increase at these boundaries is based on preliminary reference Earth model [*Dziewonski and Anderson*, 1981]. The Clapeyron slope for the 410 km and 660 km discontinuities are set to 3.0 MPa/K and −1.5 MPa/K, respectively [*Akaogi*, 2007; *Tauzin and Ricard*, 2014]. When the temperature is low, the Olivine-spinel phase transition may be delayed, forming a "metastable olivine wedge" [*Kirby et al*., 1996]. Metastable olivine is incorporated as it may be important for deep earthquake generation [*Kirby et al*., 1996; *Frohlich*, 2006; *Zhan*, 2017]. The setup of the metastable olivine follows previous studies [*Schmeling et al*., 1999; *Yang et al*., 2016]. Constant parameters used in this paper are listed in Table S1 [*Chopelas and Boehler*, 1992].

3. Results

In the reference model Case 1 (Table S2 and Figure 2a), the trench retreats rapidly at a velocity of 3 cm/yr. The reference viscosity for this model is 1×10^{21} Pa s, corresponding to a Rayleigh number of 1.075×10^8. The temperature, effective viscosity, and stress within the slab are heterogeneous and evolve with time (Figure 2a). The slab dip angle varies with time. After 16 Myr, when the slab reaches and interacts with the 660 km discontinuity, the slab dip angle is shallow and the slab flattens at ~500 km and extends westward for several hundred kilometers before it descends again to the bottom of the mantle transition zone. Before the slab reaches the 660 km discontinuity, the principle compressional stress direction at intermediate depths (~200 to ~400 km depth) is mainly perpendicular to the slab surface, while when the slab reaches the 660 km discontinuity and becomes deflected, along-dip compression gradually develops at intermediate depth within the slab (Figure 2a and Video S1), consistent with previous observations and models [*Isacks and Molnar*, 1971; *Vassiliou et al*., 1984; *Gurnis and Hager*, 1988; *Alpert et al*., 2010]. The buckling and folding of the slab produce large stress inside the slab, consistent with previous deep earthquake distribution observations [*Myhill*, 2012]. Due to the buckling and folding of the slab above the 660 km discontinuity, the phase boundary beneath the slab is not flat, consistent with recent seismic observations [*Gu et al*., 2012], and suggests that the stagnant part of the subducted Pacific plate may not be flat but have small-scale perturbations. At 16, 21, and 24 Myrs, the shallow slab dip angle, flattened slab at ~500 km, and principal stress direction are generally consistent with the seismologic observations at the northern section of the IBSZ (Figures 1b and 1c).

The parameters for reference model Case 2 (Table S2 and Figure 2b) are the same as Case 1, except that the trench retreats at a smaller, 1 cm/yr, velocity. Similar to Case 1, the slab temperature, effective viscosity, and stress are heterogeneous and evolve with time (Figure 2b). Before the slab impinges upon the 660 km discontinuity, the slab dip angle, slab morphology, and principal stress direction within the slab are similar to that of Case 1. However, the slab dip angle is generally steep, and the slab curves toward the subducting plate direction after the slab interacts with the 660 km discontinuity in Case 2, in contrast to that of Case 1. At 19 Myrs, the slab morphology and principal stress directions, including the large slab dip angle, the slightly westward extension of the slab at ~550 km depth, are similar to seismic observations at the southern section of the IBSZ

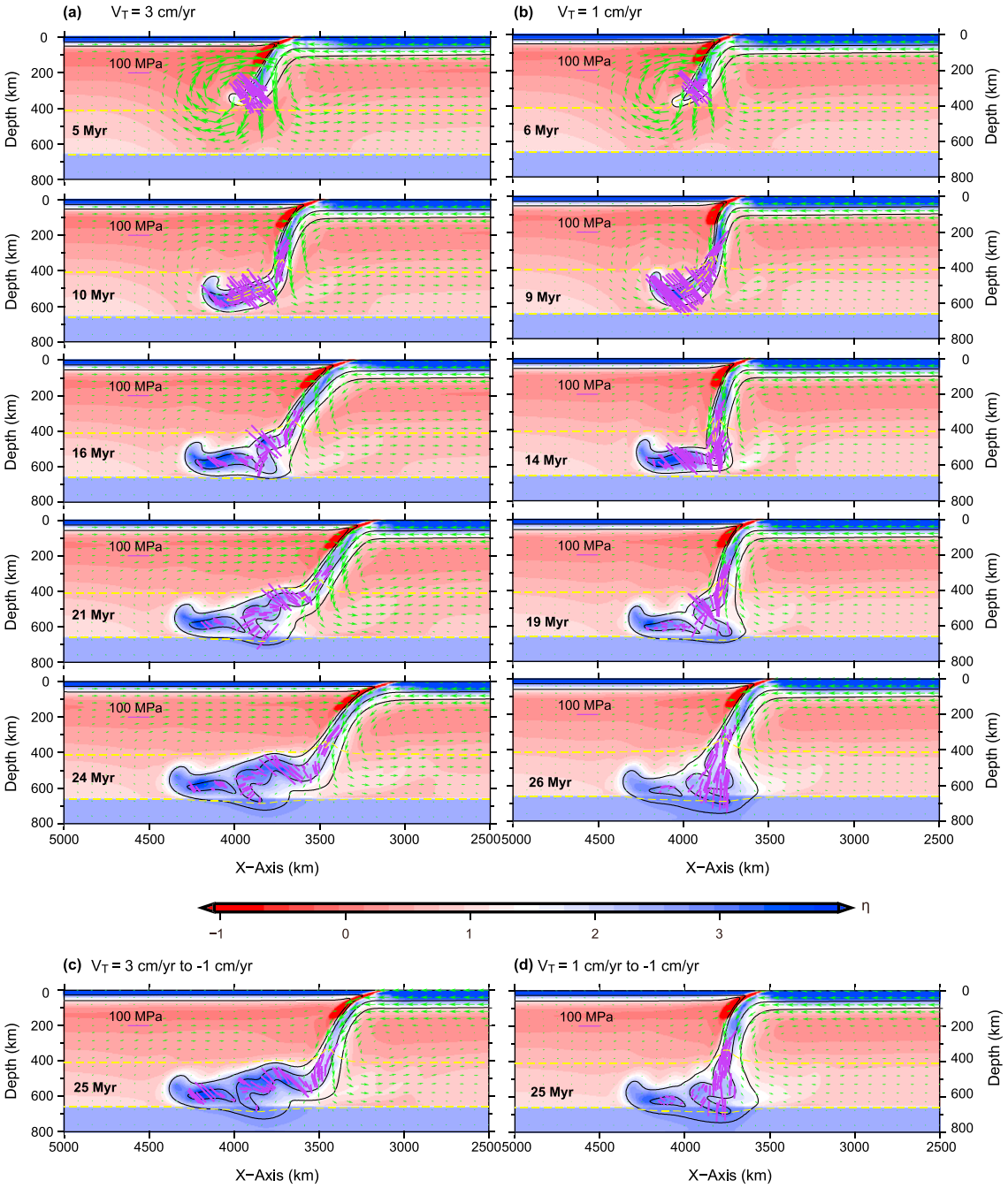

Figure 2. Slab morphology and stress evolution for the reference models (a) Case 1 and (b) Case 2, which have 3 cm/yr and 1 cm/yr trench retreat velocities, respectively. (c) Case 3 and (d) Case 4 demonstrate the influence of trench advance on slab morphology and stress state at 25 Myr. The background color represents nondimensional viscosity. The 0.6 and 0.8 temperature contours are represented by black lines. We assume that the 0.6 contour represents the cold and strong slab core and the 0.8 contour represents the shape of the cold slab that may be observed by high-resolution seismic tomography. Green arrows represent mantle flow velocity. Purple lines represent principal compressional stress with its length represent stress magnitude. Only a part of the model domain is shown to highlight structures at the subduction zone.

(Figure 1). The slab curves toward the subducting plate direction with its principal compressional stress direction oriented toward the slab. We link this slab buckling to the isolated 680 km depth Bonin Islands earthquake that lies eastward of the regionally well-defined Benioff zone and has a principal compressional stress pointing toward the predefined Benioff zone tip. Although the low-temperature, high-viscous slab core (represented by the 0.6 temperature contour) has complex buckling within

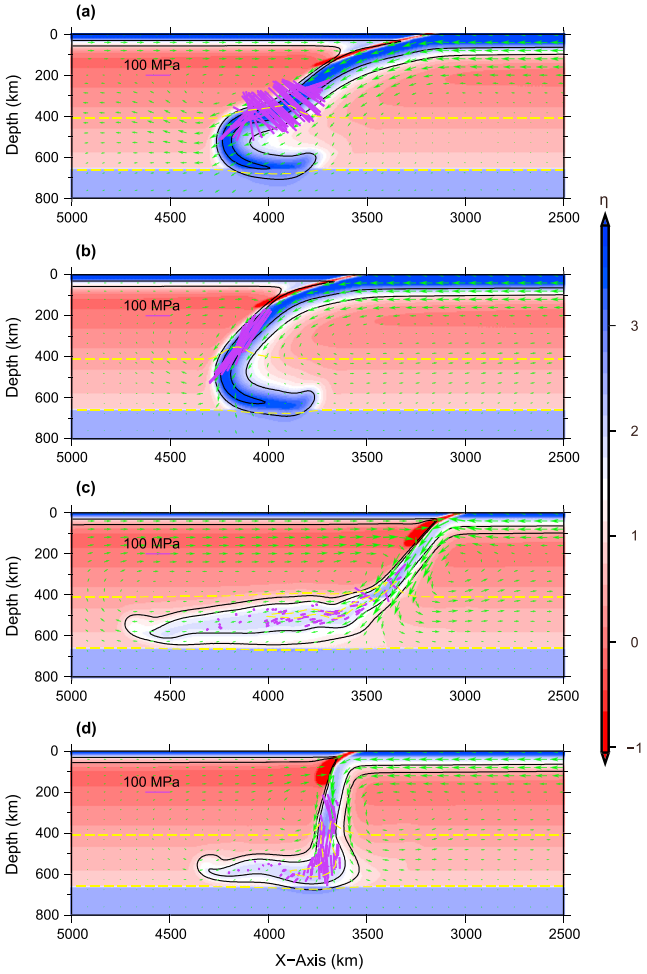

Figure 3. Slab morphology and stress at 20 Myr for pure linear viscosity models. (a) Case 5 and (b) Case 6 refer to Case 1 and Case 2, respectively, but considering only linear viscosity. (c) Case 7 and (d) Case 8 refer to Case 5 and Case 6, respectively, but the activation energy is greatly reduced.

the transition zone, the cold slab (represented by the 0.8 temperature contour, which is 270°C lower than the surrounding mantle) may only demonstrate a simple geometry (Figure 2b) in smooth tomography models, with the 30 May 2015 Bonin Islands earthquake apparently striking at the heel of the shoe-like cold slab [*Takemura et al.*, 2016; *Obayashi et al.*, 2017].

Although we do not seek a point-by-point comparison, the general consistency between the simple 2-D geodynamic models Case 1 and Case 2 and the seismic observations along the IBSZ (Figure 1) is encouraging. We further investigate the influence of recent trench advance [*Hall*, 2002; *Faccenna et al.*, 2009] on slab morphology and stress state. Case 3 and Case 4 refer to Case 1 and Case 2, respectively, but the trench motion reverses from retreat to a 1 cm/yr advance between 20 and 25 Myrs (Table S2). The change of the trench motion from retreat to advance mainly increases the slab dip angle (Figures 2c and 2d), making models more consistent with seismological observations (Figures 1b–1e).

To investigate the influence of the nonlinear viscosity on slab dynamics, we conducted two models, Case 5 and Case 6 (Figure 3). These two models have the same physical parameters as Case 1 and Case 2, except that only the linear viscosity is considered. The slabs in these linear viscosity models have very high effective viscosity and less buckling (Figures 3a and 3b). Neither the observed slab morphology nor stress directions are reproduced by these pure linear viscosity models, suggesting that nonlinear viscosity is important in reproducing the observed slab heterogeneity and stress directions. Compared to Case 5 and Case 6, we reduced the activation energy substantially in Case 7 and Case 8 (Figures 3c, 3d, and Table S2). These two weak slab models reproduce the observed slab morphology and stress directions to first order. However, reducing the activation energy in Case 7 and Case 8 greatly reduces the slab viscosity and stress in the flattened section of the slab and may hinder deep earthquake generations there.

Due to the uncertainty in plate reconstruction, we investigated different subducting plate velocity in Case 9–Case 12. Increasing the plate subduction velocity from 6 cm/yr in Case 1 and Case 2 to 8 cm/yr in Case 9 and Case 11 increases the amount of the cold slab embedded into the mantle and increases the degree of slab buckling (Figures 4a and 4c). In contrast, reducing the plate subduction velocity to 4 cm/yr in Case 10 and Case 12 reduces the amount of the cold slab material embedded into the mantle and reduces the degree of slab buckling (Figures 4b and 4d). However, the slab dip angle at shallow depth and principal stress directions are not significantly influenced by subducting plate velocity.

The subducting and overriding plate ages evolve with time, so we investigated the influence of plate ages on slab morphology and stress direction (Case 13–Case 15, Figures 4e–4g). Reducing the overriding plate age

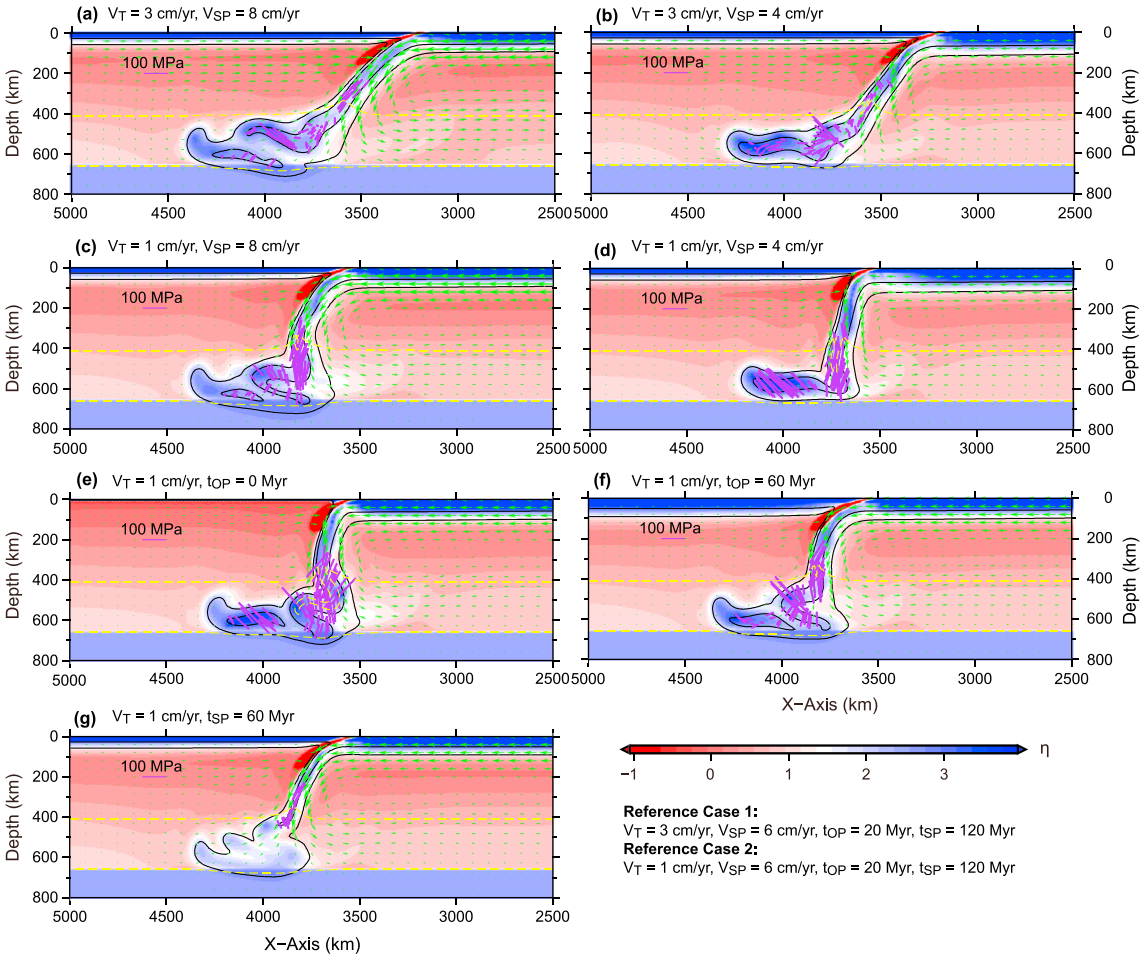

Figure 4. Slab morphology and stress at 20 Myr for different plate tectonics settings. (a–d) Varying the subducting plate velocity relative to the reference models Case 1 and Case 2. (e–g) Varying the overriding and subducting plate age relative to the reference model Case 2. The parameters of the reference models are labeled at bottom right. The varied parameters of each model relative to the reference models are labeled above each subfigure.

from 20 Myrs in Case 2 to 0 Myrs in Case 13 increases the slab dip angle and reduces the slab temperature with a large metastable olivine wedge developing inside the slab (Figure 4e). In contrast, increasing the overriding plate age from 20 Myrs in Case 2 to 60 Myrs in Case 14 reduces the slab dip angle moderately (Figure 4f), consistent with previous studies [*Rodríguez-González et al.*, 2012]. Reducing the subducting plate age from 120 Myrs in Case 2 to 60 Myrs in Case 15 significantly increases the slab temperature, reduces the stress within the slab, and hinders the generation of deep earthquakes. Influences of other physical parameters (activation energy, viscosity jump across the 660 km discontinuity, metastable olivine transitional temperature, and mantle convection Rayleigh number) on slab morphology, temperature, and stress distributions can be found in the supporting information.

4. Discussion and Conclusion

We investigated the influence of trench motion velocity on slab morphology and link it with the observed slab morphology variation along the Izu-Bonin subduction zone. Investigations confirm previous suggestions that trench retreat velocity is a key factor influencing slab dynamics [*Christensen*, 1996; *Schellart*, 2005; *Čížková and Bina*, 2013]. The slab often lies horizontally within the transition zone when the trench retreats rapidly while folding and buckling when the trench retreats slowly [*Christensen*, 1996; *Schellart*, 2005; *Faccenna et al.*, 2009; *Čížková and Bina*, 2013; *Agrusta et al.*, 2017]. Comparisons between Case 1 and Case 2 and seismic observations suggest that the observed slab morphology variations along the Izu-Bonin subduction zone can be explained by a southward reduction in the trench retreat rate [*van der Hilst and Seno*, 1993]. However,

self-consistent dynamic models accounting for time-varying trench motion history [*Faccenna et al*., 2009; *Čížková and Bina*, 2015; *Yang et al*., 2016] are needed in the future.

Zhao et al. [2017] suggested a simple slab geometry with the Pacific slab penetrating into the lower mantle without buckling based on their *P* wave tomography. In contrast, we suggest slab buckling as the explanation for the 2015 Bonin Islands deep earthquake location and principal stress direction. The horizontal width of the continuous buckling section is usually less than ~300 km in our slow slab retreat models (Figures 2b, 2d, and 4), not inconsistent with tomography results [*Zhao et al*., 2017]. Although the slightly westward flattening of the Benioff zone (Figure 1d) gives some support for slab buckling, more seismic investigations in regions around the 2015 Bonin Islands earthquake is needed to test the slab buckling model.

Deep earthquakes are often regarded as occurring within the cold core of the subducted slabs [*Kirby et al*., 1996; *Frohlich*, 2006], delineating Benioff zones. However, there are occasionally some isolated deep earthquakes that are not obviously connected with any known Benioff zones, although in tomographic images, they may lie within high seismic-velocity regions [*Engdahl et al*., 1995]. The mechanism for the formation of these isolated deep events is unclear. We suggest that the slab is essentially heterogeneous, and isolated deep earthquakes may lie within some isolated cold, strong, and high-stress blocks that are connected with Benioff zones with high-temperature and low-viscosity (but may be still colder and more viscous than the surrounding mantle) belts. Although the stress within the isolated blocks is usually low (e.g., Figure 2a after 10 Myrs), it may also be high in some cases (e.g., Figures 4e and S2d), providing a natural explanation for the small number of isolated deep earthquakes. Although our models demonstrate the inherent heterogeneity within the subducted slabs, we suggest that the slab heterogeneity would be more obvious when ultrahigh resolution [*Garel et al*., 2014] and more realistic rheology are considered.

Our investigation suggests that nonlinear viscosity plays key roles in reproducing the slab heterogeneity and observed stress direction. When only the linear viscosity is considered, the slab morphology and stress direction can only be reproduced by reducing the slab viscosity (activation energy), potentially at least partly explaining the low activation energy and weak slabs previously inferred [*Moresi and Gurnis*, 1996; *Yang and Gurnis*, 2016].

Due to the inverse relationship between strain rate (velocity gradient) and viscosity, the high effective viscosity and stress usually correspond to low strain rate. This appears to be contradicted by the occurrence of shallow earthquakes in regions with large strain rates (e.g., plate margins). We suggest that the low strain rate only acts to keep the slab as low temperature and high viscosity in the transition zone, while other processes, e.g., transformational faulting, dehydration embrittlement, or shear thermal instability [*Frohlich*, 2006], act to trigger the deep earthquakes at time scales of seconds to minutes.

Our preliminary investigations demonstrate that geodynamic models consistent with regional plate reconstructions can reproduce the observed slab stress and morphology variations along the Izu-Bonin subduction zone, suggesting that plate tectonics and mantle flow over the past tens of million years controls slab morphology, stress, temperature distributions, and the location and focal mechanism of deep earthquakes in this region. Subduction is essentially 3D with rapid along-trench variations in the Izu-Bonin-Mariana subduction zone (Figure 1). *P* wave tomography suggests that the Pacific Plate splits at ~28°N, slightly north of the 2015 Bonin Islands earthquake [*Zhao et al*., 2017]. That our 2-D models can reproduce the observed slab morphology and stress distribution to the first order suggest that slab tear has limited influences on deep earthquakes (including the 2015 Bonin Islands earthquake) in this region. However, 3-D mantle convection models are needed in the future to better understand the influence of along-trench variations and possible tear on slab stress distribution.

Acknowledgments

T. Y. benefitted from the discussion with Lingling Ye. We thank two anonymous reviewers for their commentary on the paper. Supported by the NSF under EAR-1247022, EAR-1600956, and EAR-1645775. The Finite element software Citcom used for model calculation can be downloaded from the CIG website https://geodynamics.org/.

References

Agrusta, R., S. Goes, and J. van Hunen (2017), Subducting-slab transition-zone interaction: Stagnation, penetration and mode switches, *Earth Planet. Sci. Lett.*, *464*, 10–23.

Akaogi, M. (2007), Phase transitions of minerals in the transition zone and upper part of the lower mantle, *Geol. Soc. Am. Spec. Pap.*, *421*, 1–13, doi:10.1130/2007.2421(01).

Alpert, L., T. Becker, and I. Bailey (2010), Global slab deformation and centroid moment tensor constraints on viscosity, *Geochem., Geophys., Geosyst.*, *11*, Q12006, doi:10.1029/2010GC003301.

Amante, C., and B. W. Eakins (2009), ETOPO1 1 arc-minute global relief model: Procedures, data sources and analysis, edited, NOAA Tech. Mem. NESDIS NGDC-24, Natl. Geophys. Data Cent., NOAA, doi:10.7289/V5C8276M.

Bird, P. (2003), An updated digital model of plate boundaries, *Geochem., Geophys., Geosyst.*, *4*(3), 1027, doi:10.1029/2001GC000252.
Čížková, H., and C. R. Bina (2013), Effects of mantle and subduction-interface rheologies on slab stagnation and trench rollback, *Earth Planet. Sci. Lett.*, *379*, 95–103, doi:10.1016/j.epsl.2013.08.011.
Čížková, H., and C. R. Bina (2015), Geodynamics of trench advance: Insights from a Philippine-Sea-style geometry, *Earth Planet. Sci. Lett.*, *430*, 408–415.
Chopelas, A., and R. Boehler (1992), Thermal expansivity in the lower mantle, *Geophys. Res. Lett.*, *19*(19), 1983–1986, doi:10.1029/92GL02144.
Christensen, U. R. (1996), The influence of trench migration on slab penetration into the lower mantle, *Earth Planet. Sci. Lett.*, *140*(1), 27–39.
Dziewonski, A. M., and D. L. Anderson (1981), Preliminary reference Earth model, *Phys. Earth Planet. Inter.*, *25*(4), 297–356.
Engdahl, E., R. Van der Hilst, and J. Berrocal (1995), Imaging of subducted lithosphere beneath South America, *Geophys. Res. Lett.*, *22*(16), 2317–2320, doi:10.1029/95GL02013.
Engdahl, E. R., R. van der Hilst, and R. Buland (1998), Global teleseismic earthquake relocation with improved travel times and procedures for depth determination, *Bull. Seismol. Soc. Am.*, *88*(3), 722–743.
Faccenna, C., E. Di Giuseppe, F. Funiciello, S. Lallemand, and J. Van Hunen (2009), Control of seafloor aging on the migration of the Izu–Bonin–Mariana trench, *Earth Planet. Sci. Lett.*, *288*(3), 386–398.
Frohlich, C. (2006), *Deep Earthquakes*, pp. 252–304, Cambridge Univ. Press, Cambrige, U. K.
Garel, F., S. Goes, D. Davies, J. H. Davies, S. C. Kramer, and C. R. Wilson (2014), Interaction of subducted slabs with the mantle transition-zone: A regime diagram from 2-D thermo-mechanical models with a mobile trench and an overriding plate, *Geochem., Geophys., Geosyst.*, *15*, 1739–1765, doi:10.1002/2014GC005257.
Gu, Y. J., A. Okeler, and R. Schultz (2012), Tracking slabs beneath northwestern Pacific subduction zones, *Earth Planet. Sci. Lett.*, *331*, 269–280.
Gurnis, M., and B. H. Hager (1988), Controls of the structure of subducted slabs, *Nature*, *335*(6188), 317–321.
Hall, R. (2002), Cenozoic geological and plate tectonic evolution of SE Asia and the SW Pacific: Computer-based reconstructions, model and animations, *J. Asian Earth Sci.*, *20*(4), 353–431.
Hayes, G. P., D. J. Wald, and R. L. Johnson (2012), Slab1.0: A three-dimensional model of global subduction zone geometries, *J. Geophys. Res.*, *117*, B01302, doi:10.1029/2011JB008524.
Hebert, L. B., P. Antoshechkina, P. Asimow, and M. Gurnis (2009), Emergence of a low-viscosity channel in subduction zones through the coupling of mantle flow and thermodynamics, *Earth Planet. Sci. Lett.*, *278*(3), 243–256.
Isacks, B., and P. Molnar (1971), Distribution of stresses in the descending lithosphere from a global survey of focal-mechanism solutions of mantle earthquakes, *Rev. Geophys.*, *9*(1), 103–174, doi:10.1029/RG009i001p00103.
Kirby, S. H., S. Stein, E. A. Okal, and D. C. Rubie (1996), Metastable mantle phase transformations and deep earthquakes in subducting oceanic lithosphere, *Rev. Geophys.*, *34*(2), 261–306, doi:10.1029/96RG01050.
Kuge, K. (2016), The 30 May 2015 Bonin deep earthquake and the 660-km discontinuity around its source region, AGU Ann. Meet., edited, San Francisco, Calif.
Leng, W., and S. Zhong (2008), Viscous heating, adiabatic heating and energetic consistency in compressible mantle convection, *Geophys. J. Int.*, *173*(2), 693–702.
Lundgren, P., and D. Giardini (1994), Isolated deep earthquakes and the fate of subduction in the mantle, *J. Geophys. Res.*, *99*(B8), 15,833–15,842, doi:10.1029/94JB00038.
Miller, M., A. Gorbatov, and B. Kennett (2005), Heterogeneity within the subducting Pacific slab beneath the Izu–Bonin–Mariana arc: Evidence from tomography using 3D ray tracing inversion techniques, *Earth Planet. Sci. Lett.*, *235*(1), 331–342.
Miller, M., B. Kennett, and V. Toy (2006), Spatial and temporal evolution of the subducting Pacific plate structure along the western Pacific margin, *J. Geophys. Res.*, *111*, B02401, doi:10.1029/2005JB003705.
Mitrovica, J., and A. Forte (2004), A new inference of mantle viscosity based upon joint inversion of convection and glacial isostatic adjustment data, *Earth Planet. Sci. Lett.*, *225*(1), 177–189.
Moresi, L., and M. Gurnis (1996), Constraints on the lateral strength of slabs from three-dimensional dynamic flow models, *Earth Planet. Sci. Lett.*, *138*(1), 15–28.
Moresi, L., S. Zhong, and M. Gurnis (1996), The accuracy of finite element solutions of Stokes's flow with strongly varying viscosity, *Phys. Earth Planet. Inter.*, *97*(1), 83–94.
Myhill, R. (2012), Slab buckling and its effect on the distributions and focal mechanisms of deep-focus earthquakes, *Geophys. J. Int.*, doi:10.1093/gji/ggs1054.
Obayashi, M., Y. Fukao, and J. Yoshimitsu (2017), Unusually deep Bonin earthquake of 30 May 2015: A precursory signal to slab penetration?, *Earth Planet. Sci. Lett.*, *459*, 221–226.
Okal, E., and S. H. Kirby (2016), The large Bonin deep event of 30 May 2015: Seismogenesis in a detached and fragmented slab, paper presented at EGU General Assembly Conf. Abstr., Vienna.
Porritt, R. W., and S. Yoshioka (2016), Slab pileup in the mantle transition zone and the 30 May 2015 Chichi-jima earthquake, *Geophys. Res. Lett.*, *43*, 4905–4912, doi:10.1002/2016GL068168.
Rodríguez-González, J., A. M. Negredo, and M. I. Billen (2012), The role of the overriding plate thermal state on slab dip variability and on the occurrence of flat subduction, *Geochem., Geophys., Geosyst.*, *13*, Q01002, doi:10.1029/02011GC003859.
Schellart, W. (2005), Influence of the subducting plate velocity on the geometry of the slab and migration of the subduction hinge, *Earth Planet. Sci. Lett.*, *231*(3), 197–219.
Schmeling, H., R. Monz, and D. C. Rubie (1999), The influence of olivine metastability on the dynamics of subduction, *Earth Planet. Sci. Lett.*, *165*(1), 55–66.
Stadler, G., M. Gurnis, C. Burstedde, L. C. Wilcox, L. Alisic, and O. Ghattas (2010), The dynamics of plate tectonics and mantle flow: From local to global scales, *Science*, *329*(5995), 1033–1038.
Stegman, D., R. Farrington, F. Capitanio, and W. Schellart (2010), A regime diagram for subduction styles from 3-D numerical models of free subduction, *Tectonophysics*, *483*(1), 29–45.
Takemura, S., T. Maeda, T. Furumura, and K. Obara (2016), Constraining the source location of the 30 May 2015 (M_w 7.9) Bonin deep-focus earthquake using seismogram envelopes of high-frequency *P* waveforms: Occurrence of deep-focus earthquake at the bottom of a subducting slab, *Geophys. Res. Lett.*, *43*, 4297–4302, doi:10.1002/2016GL068437.
Tauzin, B., and Y. Ricard (2014), Seismically deduced thermodynamics phase diagrams for the mantle transition zone, *Earth Planet. Sci. Lett.*, *401*, 337–346.
van der Hilst, R., and T. Seno (1993), Effects of relative plate motion on the deep structure and penetration depth of slabs below the Izu-Bonin and Mariana island arcs, *Earth Planet. Sci. Lett.*, *120*(3), 395–407.

van Hunen, J., A. P. van den Berg, and N. J. Vlaar (2000), A thermo-mechanical model of horizontal subduction below an overriding plate, *Earth Planet. Sci. Lett.*, *182*(2), 157–169.

Vassiliou, M., B. Hager, and A. Raefsky (1984), The distribution of earthquakes with depth and stress in subducting slabs, *J. Geodyn.*, *1*(1), 11–28.

Von Hagke, C., M. Philippon, J.-P. Avouac, and M. Gurnis (2016), Origin and time evolution of subduction polarity reversal from plate kinematics of Southeast Asia, *Geology*, *44*(8), 659–662.

Wei, W., J. Xu, D. Zhao, and Y. Shi (2012), East Asia mantle tomography: New insight into plate subduction and intraplate volcanism, *J. Asian Earth Sci.*, *60*, 88–103.

Wu, J., J. Suppe, R. Lu, and R. Kanda (2016), Philippine Sea and East Asian plate tectonics since 52 Ma constrained by new subducted slab reconstruction methods, *J. Geophys. Res. Solid Earth*, *121*, 4670–4741, doi:10.1002/2016JB012923.

Yang, T., and M. Gurnis (2016), Dynamic topography, gravity and the role of lateral viscosity variations from inversion of global mantle flow, *Geophys. J. Int.*, *207*(2), 1186–1202.

Yang, T., M. Gurnis, and S. Zahirovic (2016), Slab avalanche-induced tectonics in self-consistent dynamic models, *Tectonophysics*, doi:10.1016/j.tecto.2016.1012.1007.

Ye, L., T. Lay, Z. Zhan, H. Kanamori, and J.-L. Hao (2016), The isolated ~680 km deep 30 May 2015 M_W 7.9 Ogasawara (Bonin) Islands earthquake, *Earth Planet. Sci. Lett.*, *433*, 169–179.

Zhan, Z. (2017), Gutenberg–Richter law for deep earthquakes revisited: A dual-mechanism hypothesis, *Earth Planet. Sci. Lett.*, *461*, 1–7.

Zhao, D., M. Fujisawa, and G. Toyokuni (2017), Tomography of the subducting Pacific slab and the 2015 Bonin deepest earthquake (M_w 7.9), *Sci. Rep.*, *7*, 44487, doi:10.1038/srep44487.

Zhong, S. (2006), Constraints on thermochemical convection of the mantle from plume heat flux, plume excess temperature, and upper mantle temperature, *J. Geophys. Res.*, *111*, B04409, doi:10.1029/2005JB003972.

Zhong, S., and M. Gurnis (1995), Mantle convection with plates and mobile, faulted plate margins, *Science*, *267*(5199), 838.

Zhong, S., M. Gurnis, and L. Moresi (1998), Role of faults, nonlinear rheology, and viscosity structure in generating plates from instantaneous mantle flow models, *J. Geophys. Res.*, *103*(B7), 15,255–15,268, doi:10.1029/98JB00605.